Research on Engineering Structures & Materials
www.jresm.org
Research Group

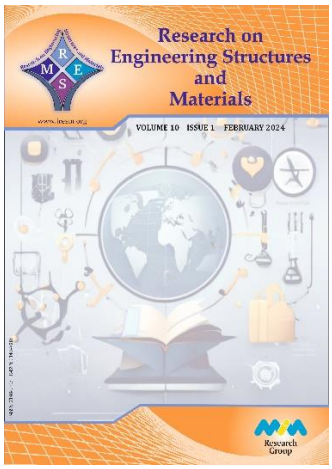

Parametric study on the effect of temperature on properties of engineered cementitious composites using induction furnace slag as a partial replacement for river sand

S Naveena, Govardhan Bhat

Online Publication Date: 31 December 2023
URL: http://www.jresm.org/archive/resm2023.36ma0824rs.html
DOI: http://dx.doi.org/10.17515/resm2023.36ma0824rs
Journal Abbreviation: *Res. Eng. Struct. Mater.*

To cite this article
Naveena S, Bhat G. Parametric study on the effect of temperature on properties of engineered cementitious composites using induction furnace slag as a partial replacement for river sand. *Res. Eng. Struct. Mater.*, 2024; 10(3): 897-915.

Research on Engineering Structures & Materials
www.jresm.org
Research Group

Research Article

Parametric study on the effect of temperature on properties of engineered cementitious composites using induction furnace slag as a partial replacement for river sand

S Naveen[a,*], Govardhan Bhat[b]

Department of Civil Engineering, NIT Raipur, Chhattisgarh-492010, India

Article Info

Article history:

Received 24 Aug 2023
Accepted 31 Dec 2023

Keywords:

River sand;
Induction furnace steel slag;
Engineered cementitious composites;
Elevated temperatures;
Normalized strength;
Normalized UPV

Abstract

This paper studies the effect of temperature on Engineered Cementitious Composites (ECC) properties using induction furnace slag (SS) as a partial replacement for river sand (RS). Replacement percentages are between 5 and 65%, with an increment of 15% by dry weight of RS having various particle sizes (2.36 mm, 1.18 mm and 0.6 mm). The cubes are subjected to various temperatures (200, 400, 600 and 800^{0}C) in a muffle furnace. After heating, visual observations and strength deterioration of RS and SS ECC are assessed. The extent of postfire damage is determined using the UPV test. SEM and XRD are used to identify the changes in the microscopy morphology and the chemical compositions. It is clear from the test findings that with SS partially replacing RS, the heat insulation capacity of ECC is enhanced. Based on test results, the ECC up to 50% SS as an RS alternative performs better at all temperature exposures.

1. Introduction

Engineered cementitious composites (ECC), composed of cement, fly ash, fine aggregate, chemical admixture, water and fibres, were developed by Victor Li to overcome the brittleness of traditional cement-based materials. Especially as a fine aggregate micro-silica sand used in ECC [1]. Sand size, amount, and roughness impact ECC's properties [2]. ECC is utilised in structural applications, including bridges, high-rise buildings, road pavements, and repair and retrofitting structures [3]. It can also be used in earthquake-resisting structures [4]. ECC enhances structure service life, which reduces maintenance and repair costs [5]. Furthermore, ECC performs much better than conventional concrete when exposed to chemical attacks and various temperatures.

Fire generally has an impact on structural behaviour at various temperatures. Including Polyvinyl alcohol (PVA) fibres in ECC can reduce explosive spalling at various temperatures [6]. Many researchers have studied the performance of ECC at various temperatures, and its performance depends on the materials used (fly ash, fibres, and aggregate). The existing literature on ECC at various temperatures shows that micro silica sand of size < 300 microns is used as fine aggregate [7–9]. Instead of using micro silica sand, quartz sand characterises the behaviour of fibre-reinforced cementitious composites at various temperatures [10]. He et al. [11] investigated high-strength ECC at various temperatures, in which River Sand (RS) with a 2 mm particle size is used. According to

*Corresponding author: naveence.viit@gmail.com
[a] orcid.org/0000-0002-5555-9691; [b] orcid.org/0000-0002-8693-1918
DOI: http://dx.doi.org/10.17515/resm2023.36ma0824rs

experimental studies, the strength loss in high-strength ECC is less than in ECC with normal strength. Mohammed et al. [12] performed a study on nano-silica-modified self-consolidating ECC at various temperatures using fine aggregate as RS with 450 microns size. The residual characteristics of nano-silica-modified self-consolidating ECC decreased as temperature increased from 200^{0}C to 400^{0}C. Cao et al. [13] explored the bonding characteristics of existing concrete and steel-basalt hybrid fibre-reinforced cementitious composite (SBFRCC) at various temperatures. The fine aggregate employed in this investigation is RS with a 0.6mm particle size. The test results show that the SBFRCC performed better at high temperatures than existing concrete. The earlier studies focused on ECC's performance with micro silica sand and RS as a fine aggregate at various temperatures. Still, its performance using steel industry by-products as a fine aggregate at various temperatures is not explored.

The most crucial strategy for resolving sustainability issues in the construction sector is effectively transforming industrial by-products into useful concrete materials. Such an approach also protects the environment from harmful solid waste dumped from industries. Ferrites and Calcium silicates combined with the fused oxides of aluminium, calcium, iron, manganese, and magnesium form a non-metallic steel slag [14]. The expansion in concrete is caused by the Free lime and periclase in SS [15]. Studies related to the tests and methods for volume stability are developed. Mehta et al. described autoclave test evolution history as a critical assessment of its current state, and the widely used performance tests for cement soundness are described [16]. Hydration of crystalline magnesia (periclase) is a primary reason for such volume change. The microstructure and expansive behaviour of cement with varying Mgo contents and autoclave expansions are explored [17]. The volume stability of SS aggregate can be assessed by testing the free lime content [18]. Lun et al. developed techniques for enhancing the volume stability of SS as a fine aggregate [19]. Weathering is also the best approach for the volume stability of SS.

The characteristics of the SS produced may vary based on furnace type, processing methods and raw materials used [20]. Induction furnaces have Induction Furnace Steel Slag (SS), a good substitute due to their efficient operation and clean manufacturing process [21]. Over 600 Induction furnace plants exist in India alone, each producing over 15,000 tonnes of slag annually [14]. Netinger Grubesa et al. [22] demonstrated that concrete properties with steel slag are similar to the dolomite concrete up to 600^{0}C. Liang et al. [23] implemented ultra-high-performance concrete with 69% residual strength after being subjected to 1000^{0}C with SS as fine aggregate. Jihad Miah et al. [24] observed that the strength reduction at various temperatures increases when sand is replaced by 100% Steel slag powder. The previous literature focused on cement mortar/concrete with SS as fine aggregate at various temperatures. Still, studies related to ECC behaviour at various temperatures with SS aggregate are not covered in the literature. The properties of ECC with SS as a partial substitute material for RS with 5%, 20%, 35%, 50% and 65% having various particle sizes at various temperatures (200, 400, 600 and 800^{0}C) are evaluated. ECC's chemical composition and microstructural properties are identified with SEM and XRD. The results of ECC with SS at elevated temperatures are beneficial for ensuring stable fire resistance of the structural elements.

2. Experimental Work

2.1. Materials

2.1.1 Cement

As per IS 269: 2015, Ordinary Portland Cement is utilized in all the mixes. The test findings for cement are given in Table 1, confirming the IS: 269: 2015 specifications.

Table 1. Cement properties

Properties	Values	As per IS:269-2015
Normal consistency	30%	-
Initial setting time	147	>30 min
Final setting time	257	< 600 min
Fineness		
a. Dry sieving	4	Less than 10%
b. Blain's air permeability	310.7	More than 225 m^2/kg
Specific gravity	3.04	-

2.1.2 Fly Ash

Fly ash (FA) confirms the requirements of IS 3812 (Part-1): 2003. The chemical composition of the FA from Energy Dispersive Spectroscopy (EDS) is shown in Table 2.

Table 2. Chemical composition of fly ash from EDS

Chemical composition	Oxide (%)
SiO_2	62.73
Al_2O_3	29.17
Fe_2O_3	3.17
MgO	0.68
CaO	0.82
Na_2O	-
K_2O	1.23

2.1.3 Fine Aggregate

RS and SS are used as fine aggregates in ECC and classified as Zone-II, according to IS 383: 2016. The fine aggregate chemical composition is shown in Table 3. The distribution of particle sizes is shown in Fig. 1. Both RS and SS, particle size distributions, are within the upper and lower bound limit. In Table 4, the engineering properties of RS and SS are listed. SEM images of RS and SS particles are shown in Fig. 2, which indicate that the particles of SS are relatively rough and angular compared to those of RS particles.

Table 3. Chemical composition of fine aggregate (RS and SS) by EDS analysis

Chemical composition	Oxide percentage in RS (%)+Oxide percentage in SS (%)	
SiO_2	75.11	49.86
TiO_2	-	0.48
Cr_2O_3	-	0.2
Al_2O_3	13.18	15.95
Fe_2O_3	4.92	24.66
Mn	-	1.92
MgO	0.33	0.76
CaO	1.34	4.52
Na_2O	-	0.95
K_2O	5.09	0.65

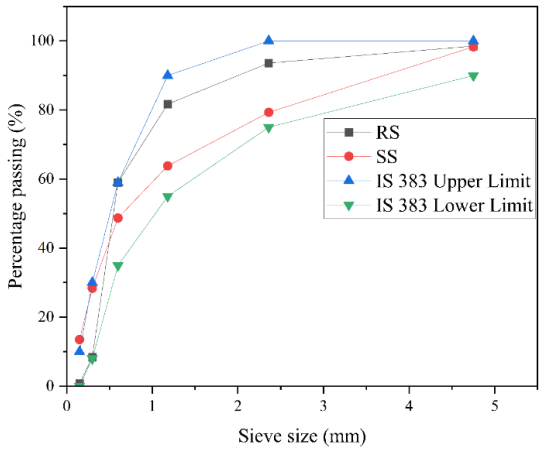

Fig. 1. Distribution of RS and SS particle sizes

Table 4. Fine aggregate Properties

Description	RS	SS
Zone	II	II
Fineness modulus	2.58	2.68
Specific gravity	2.56	2.45

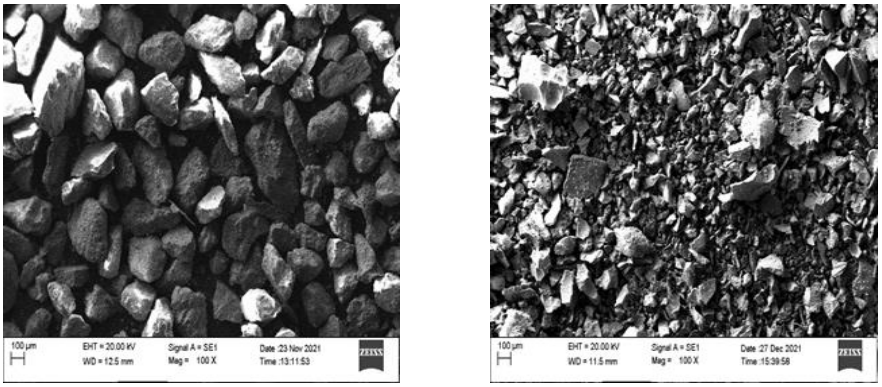

(a) (b)

Fig. 2. SEM images of (a) RS and (b) SS

2.1.4 Polyvinyl Alcohol (PVA) Fibres

In the current study, PVA fibres coated with a 1.2% hydrophobic oiling agent are utilized, and their features are listed in Table 5. The image of PVA fibres is depicted in Fig. 3. Fibres may decrease the flowability because they may restrict the smooth flow and movement of sand particles and cement paste.

Table 5. Manufacturer-specified properties of PVA fibres

Properties	PVA fibres
Length	12 mm
Fracture elongation	6 %
Modulus of Elasticity	40 GPa
Density	1.30 g/cm^3
Diameter	40 µm

Fig. 3. PVA fibres

2.1.5 Superplasticizer (SP)

Polycarboxylic acid-type superplasticizer is deployed to enhance the flowability and prevents fibre agglomeration, thus regulating the distribution of fibre in the mix.

2.2 Mix Proportions

In the ECC mix design, the mix proportion is adopted per Li et al., [25] as shown in Table 6. The standard M45 ECC mix is the most common ECC mix used in practical applications, which has an FA-to-cement ratio of 1.2. It also enhances the flowability of fresh ECC and improves mechanical properties after 90 days. The materials used in preparing ECC mixes are fixed, and the amount of SS varies as a replacement of (5%, 20%, 35%, 50%, and 65%) RS. Based on the past literature available on SS, the percentages are fixed. However, for each percentage, RS or SS particle sizes vary. All mixes are given a specific identity, such as E1, E2 and E3 for control mixes without SS at 2.36 mm, 1.18 mm and 0.60 mm particle sizes. At the same time, E4 - E18 is used for mixes containing 5%, 20%, 35%, 50%, and 65% SS with various particle sizes, respectively. Due to the larger aggregate size in the present research, a higher amount of fibre may lead to fibre clumping; hence, it is only employed at 1% of the volume for all the mixes. Based on the local ingredient conditions to ensure proper fibre dispersion, the superplasticizer and water content are finalized by conducting a marsh cone test. To investigate the influence of SS percentage and size on the properties of ECC, the same constituent proportions but with various particle sizes (2.36mm, 1.18 mm and 0.6 mm) for varying replacement percentages of RS by SS are prepared.

Table 6. Different mix proportions

Mix	Cement	Fly ash	River sand	Steel Slag	Water	SP	PVA fibre, vol%

E1	1	1.2	0.8	-	0.64	0.015	1
E2	1	1.2	0.8	-	0.64	0.015	1
E3	1	1.2	0.8	-	0.64	0.015	1
E4	1	1.2	0.76	0.04	0.64	0.015	1
E5	1	1.2	0.76	0.04	0.64	0.015	1
E6	1	1.2	0.76	0.04	0.64	0.015	1
E7	1	1.2	0.64	0.16	0.64	0.015	1
E8	1	1.2	0.64	0.16	0.64	0.015	1
E9	1	1.2	0.64	0.16	0.64	0.015	1
E10	1	1.2	0.52	0.28	0.64	0.015	1
E11	1	1.2	0.52	0.28	0.64	0.015	1
E12	1	1.2	0.52	0.28	0.64	0.015	1
E13	1	1.2	0.4	0.4	0.64	0.015	1
E14	1	1.2	0.4	0.4	0.64	0.015	1
E15	1	1.2	0.4	0.4	0.64	0.015	1
E16	1	1.2	0.28	0.52	0.64	0.015	1
E17	1	1.2	0.28	0.52	0.64	0.015	1
E18	1	1.2	0.28	0.52	0.64	0.015	1

2.3 Test Methods

The methodology used in the current research is shown in Fig. 4. The flowability of fresh ECC is evaluated using a spread flow test after the mixing process. The ECC mix is poured into a 70.6 mm cube mould. After a day, the specimens are de-moulded and placed in water til the testing age (28 and 90 days). A muffle furnace is used for heating specimens.

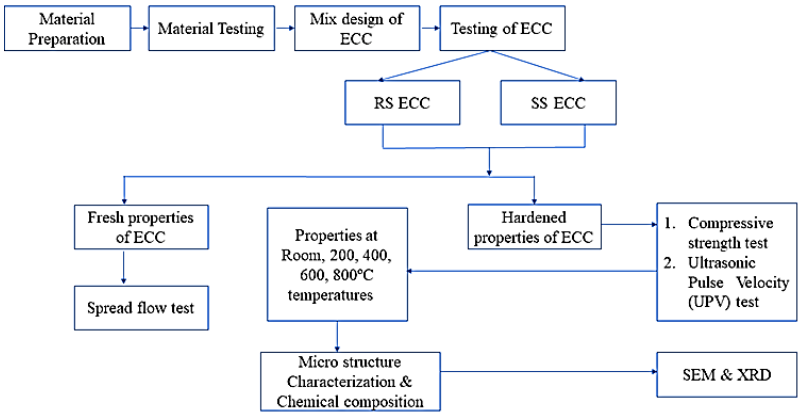

Fig. 4. Methodology for the current study

The exposure time maintained is considered from ISO 834 guidelines [26]. It is calculated based on the formula given in Eq (1), and The ISO 834 curve is shown in Fig. 5 [27]. The exposure temperatures selected from the literature are 200^{0}C, 400^{0}C, 600^{0}C, and 800^{0}C [7]. UPV and compressive strength are evaluated after the heating process. SEM and XRD are used to identify changes in microstructure and chemical composition.

$$T_f = T0 + 345 \log10 (1+8t) \quad (1)$$

Where, T_f = average "furnace" temperature, ^{0}C; T0 = initial temperature ^{0}C, and T= time, min

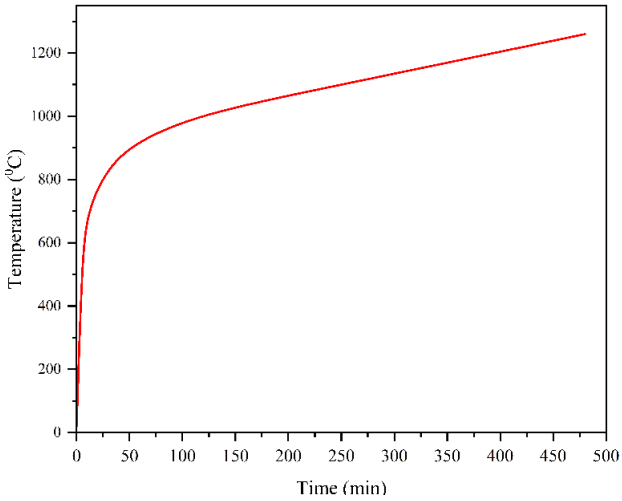

Fig. 5. ISO 834 curve

3. Results and Discussions

3.1 Spread flow test

The Flowability of fresh ECC is evaluated using a spread-flow test. Depending on the size of the employed fine aggregate, the flowability of ECC changes. Fresh ECC's plastic viscosity affects the material's characteristics [28]. So, the impact of grading on flowability needs to be evaluated. Fig. 6 shows that adding the SS marginally reduces the flowability for ECC. The flowability values of the mixes containing only RS (E1-E3) are about 210-185 mm. When RS partially replaces the SS, the flowability values are 200-135 mm for the E4-E18, respectively. The combination of fibres with SS's angular and rough surface texture (see Fig. 2b) may restrict the smooth flow. The shape of SS aggregates significantly affects flowability; while designing the mix, more care must be taken for the required w/c and proper gradation.

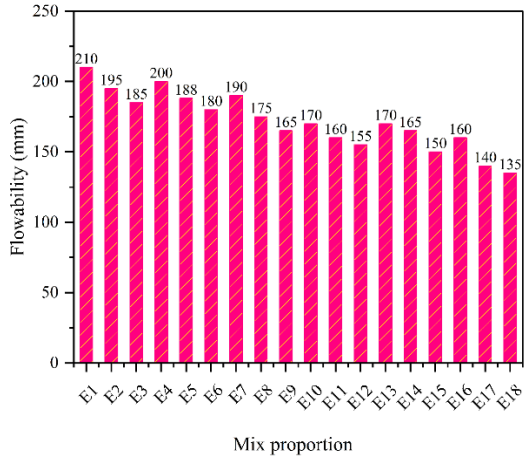

Fig. 6. ECC flowability for different mix proportions

All mixes are prepared with the same dosage of SP and water-to-binder ratio (W/b). The flowability of the SS ECC mixes is not improved Because the same dosage of SP is used for aggregates with different water absorption. However, using SP does not increase the flowability, and it is later noticed that the strength and durability are not affected by the decrease in flowability.

3.2 Compressive Strength Test

The compressive strength is determined per IS 516 standards. Fig. 7 indicated that the strength increased significantly with an increase in SS of up to 50% replacement, and after a 50% gradual decrease is observed. As compared with coarser particle mixes (E1, E4, E7, E10 and E13), the finer particle mixes (E3, E6, E9, E12 and E15) show higher strength at all curing periods.

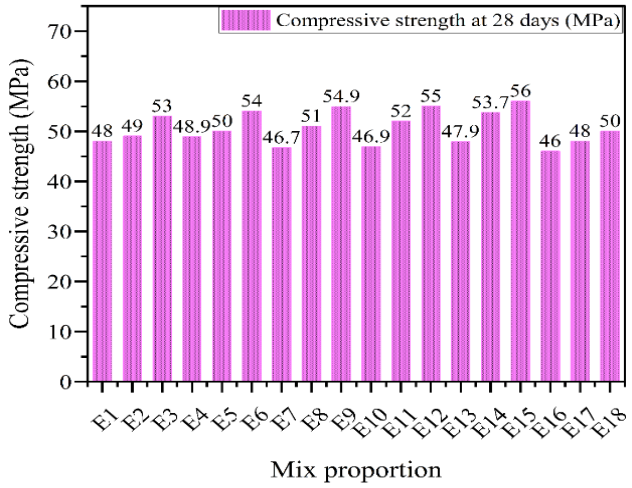

(a)

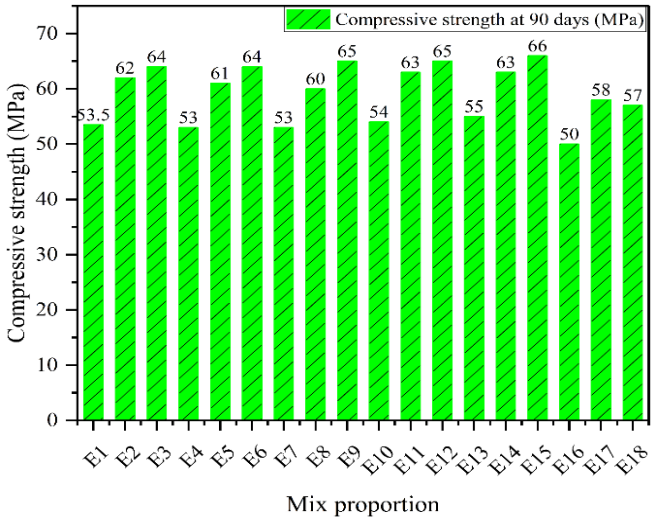

(b)

Fig. 7. ECC compressive strength for different mix proportions

Due to the larger proportion of finer particles than RS, mixes that contain 50% SS have an increase in strength, which helps in the development of a denser microstructure. Another reason is the reaction between SiO_2 and $Ca(OH)_2$. According to Table 3, SS contains about 50%SiO_2. $Ca(OH)_2$ produced on the hydration of cement can react with SiO_2 to form more C-S-H, which reduces the porosity and enhances the strength. Additionally, the SS employed in this study has a rough surface texture and an angular shape (see Fig. 2 b), which improves the bond between the aggregate and cement paste along with the reduction amount of voids [29].

3.3 UPV Test

A non-destructive experiment to check the homogeneity of a specimen is UPV. It calculates the sound wave transmission velocity inside the specimen. In Fig. 8, it is observed that ECC mixes with partial substitution of RS by SS up to 50%; the UPV increases gradually, and after that, it decreases at all curing ages—the reaction of SiO_2 with $Ca(OH)_2$. According to Table 3, SS contains about 50%SiO_2. $Ca(OH)_2$ produced on the hydration of cement can react with SiO_2 to form more C-S-H, which reduces the porosity and enhances the strength. Another reason is due to finer particles in SS, which fill the micropores in the composite; E15 exhibits the peak value in UPV.

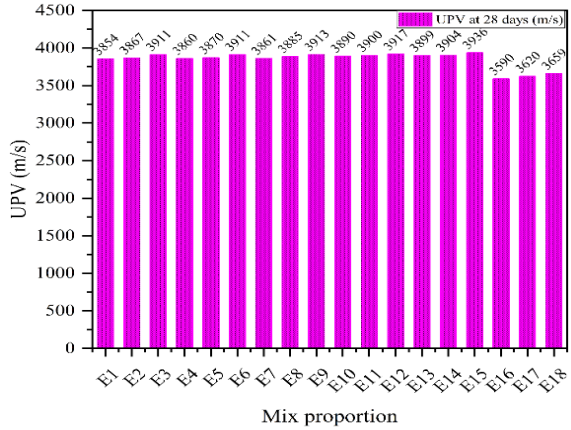

(a)

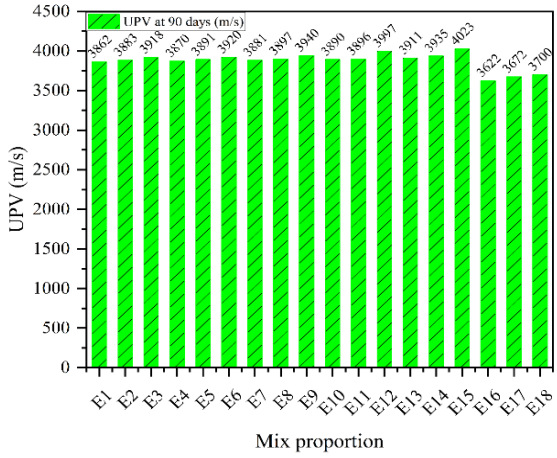

(b)

Fig. 8. ECC UPV for different mix proportions

3.4 ECC Properties at Various Temperatures

3.4.1 Appearance of the Specimen

A change in the specimen's colour is observed as a result of exposure to various temperatures, as illustrated in Fig. 9. The darker surface of RS ECC specimens at 200^{0}C results from dehydration and water evaporation. As the temperature reaches 400^{0}C, PVA fibres melt, resulting in grey. After 600^{0}C, a light grey colour indicates C-S-H gel dehydration. Yellowish grey at 800^{0}C is related to C-S-H gel decomposition. Similarly, the colour of SS ECC specimens is comparable to that of RS ECC specimens up to 600^{0}C. Grey-white after exposure to 800^{0}C is due to ECC containing SS, which has higher heat-insulation capacity and extends the time it takes for hydration products to decompose.

(a) (b)

Fig. 9. Appearance of specimens at various temperatures: (a) RS ECC (b) SS ECC

3.4.2 Compressive Strength Test

The ratio of compressive strength at various temperatures (f_{CT}) and compressive strength at 28^{0}C (f_C) is used to obtain normalized strength (f_{CT}/ f_C). The f_{CT}/ f_C of ECC at various temperatures for 28 and 90 days are indicated in Fig. 10 and Fig. 11. Fig. 10 shows that after exposure to 200^{0}C, the strength for E1, E2 and E3 is improved by 6.1%, 8.3% and 7.5% for 28 days as compared with specimens at 28^{0}C. A similar phenomenon is observed in another study [30]. It is due to the accelerated pozzolanic reaction, but for 90 days (Fig. 11), it shows a 9%, 6% and 4% reduction in strength.

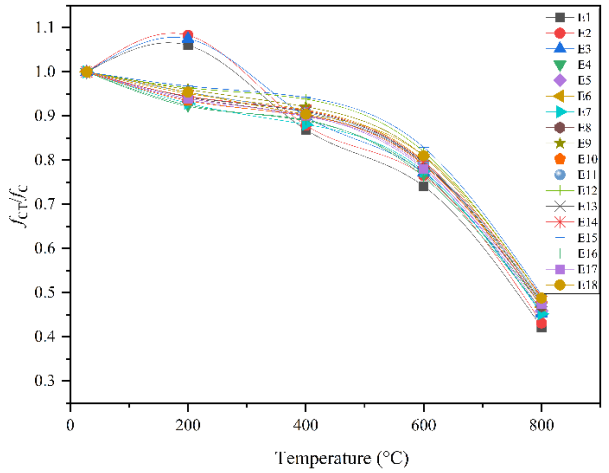

Fig. 10. ECC compressive strength at various temperatures after 28 days

When the temperature rises over 400^{0}C, the strength of ECC mixes decreases, due to the small channels from melted PVA fibres in the matrix (Fig. 18). After exposure to 600^{0}C and 800^{0}C, due to hydrates decomposition, the strength is decreased. Normalized strength for E4-E18 is higher than those of E1-E3 regardless of the curing period because of the denser structure and heat-insulation capacity of the SS [31]. As mentioned below, C-S-H would decompose at 800^{0}C, and Fig. 16 clearly shows that E3 contained significantly less C-S-H than E15. The C-S-H is responsible mainly for the ECC strength. So, the strength loss is greater when C-S-H is very low. A similar trend is observed (Fig. 11) for 90 days.

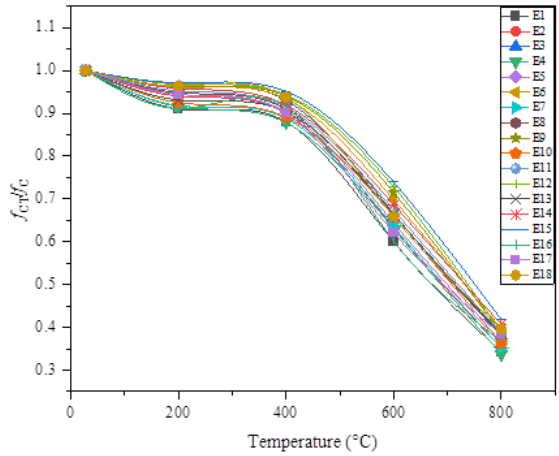

Fig. 11. ECC compressive strength at various temperatures after 90 days

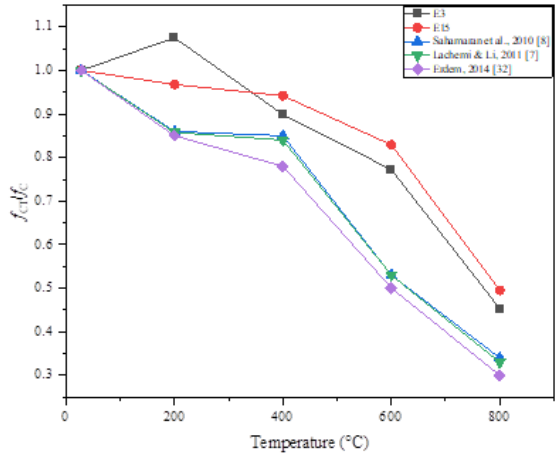

Fig. 12. Normalized compressive strength comparison with literature

The normalized compressive strength of M45 ECC obtained from the literature is compared in Fig. 12 [8][7][32]. The normalized strength of E15 is higher at all temperatures when compared to the results of earlier research. The reaction between SiO_2 and $Ca(OH)_2$. According to Table 3, SS contains about 50%SiO_2. It is well known that the silicates can react with $Ca(OH)_2$ produced during cement hydration to form additional C-S-H compounds, which reduce the porosity and enhance the strength. Another reason is that ECC containing SS, which has higher heat-insulation capacity, delays the decomposition of hydration products even at 800^{0}C.

3.4.3 UPV Test

The ratio of UPV at various temperatures (U_T) and UPV at 28^{0}C (U) is used to obtain normalized UPV (U_T/U). The U_T/U of ECC at various temperatures for 28 and 90 days are presented in Fig. 13 and Fig. 14. Up to 400^{0}C, the formation of small channels in the specimens due to the melted fibres causes the percentage variation in UPV. At high temperatures (600^{0}C and 800^{0}C), more pores are formed in ECC, extending the pulse wave travel distance and lowering the UPV values. ECC developed with SS (E4-E18) suffered less internal damage at various temperatures than ECC made with RS (E1-E3), because of the stable chemical composition of SS. However, E15 stands out best because of its denser structure and stronger heat insulation capacity.

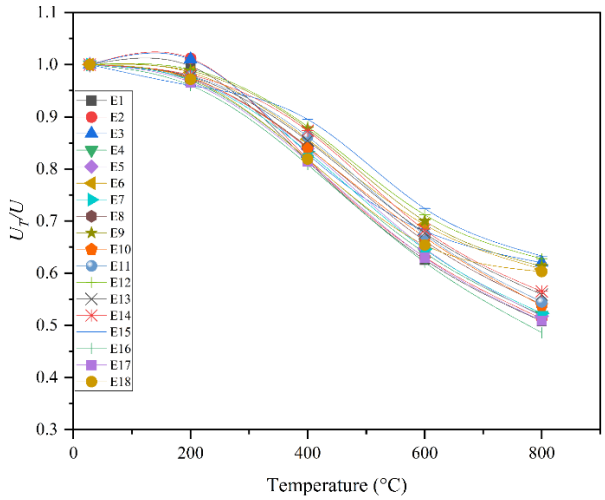

Fig. 13. ECC UPV at various temperatures after 28 days

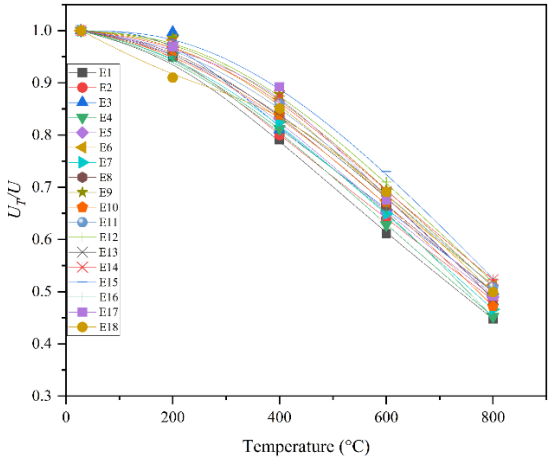

Fig. 14. ECC UPV at various temperatures after 90 days

3.4.4 Stress-Strain Curves at Various Temperatures

The stress-strain curves of E3 and E15 specimens at various temperatures (T0, T1, T2, T3 and T4 represent the 28^{0}C, 200^{0}C, 400^{0}C, 600^{0}C and 800^{0}C) at 90 days are shown in Fig.

15. The decrease of peak stress of the curves are observed for both RS and SS ECC specimens with an increase of temperature up to 800^{0}C. But, higher peak stress and strain values are observed for E15 compared to E3 at various temperatures. The peak strain is relatively high at 28^{0}C because the PVA fibres prevent cracks from forming and expanding. The PVA fibres melted at 200^{0}C, increasing the porosity. As the temperature rises, more cracks form and the peak strain is attained at a higher rate. With increased temperature, the ductile nature of both RS and SS ECC specimens becomes brittle.

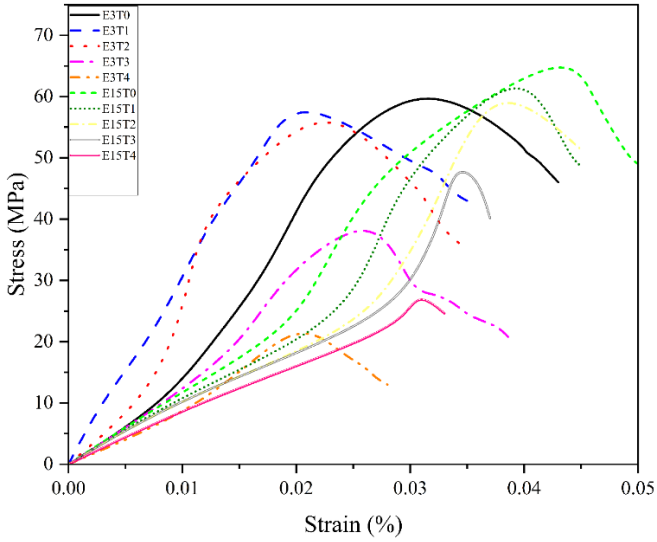

Fig. 15. Stress-strain curves at various temperatures after 90 days

3.4.5 Chemical Composition at Various Temperatures

A study on various mixes at various temperatures is conducted on cube specimens. XRD analysis is performed on the samples collected after the compressive testing process to identify the chemical composition of ECC. Among all, better properties are observed in E3 and E15. So, the XRD pattern of E3 and E15 at various temperatures is highlighted in Fig. 16. At 28^{0}C, hydration products like Calcium Silicate Hydrate (C-S-H) and Portlandite ($Ca(OH)_2$) are identified for both E3 and E15.

The dehydration process is initiated at various temperatures. For E3, at 200^{0}C, the decreased peak value of SiO_2 is observed, as indicated in Fig. 16 (a), but it increases when ECC is subjected to 400, 600 and 800^{0}C. For E15, the peak of SiO_2 is higher at 28^{0}C and becomes lower after exposure up to 800^{0}C (Fig. 16 (b)), resulting in more C-S-H gel formation than E3. The C-S-H phase is still identified at 800^{0}C for E15 and not observed for E3. At 200^{0}C and 400^{0}C, part of $Ca(OH)_2$ starts to decompose ($Ca(OH)_2 \rightarrow CaO + H_2O$), at 600^{0}C and 800^{0}C, is not observed in E3 and E15. In general, Ca(OH)2 decomposition is completed at about 530^{0}C [33]. At 800^{0}C, Dicalcium Silicate (Ca_2SiO_4) and Tricalcium Silicate (Ca_3SiO_5) are identified, which are formed due to hydration products decomposition for E3, along with Ca_2SiO_4 and Ca_3SiO_5, the Magnesium Ferrite ($MgFe_2O_4$) is found for E15. The $MgFe_2O_4$ is formed due to a chemical reaction between magnesium oxide (MgO) and ferric oxide (Fe_2O_3).

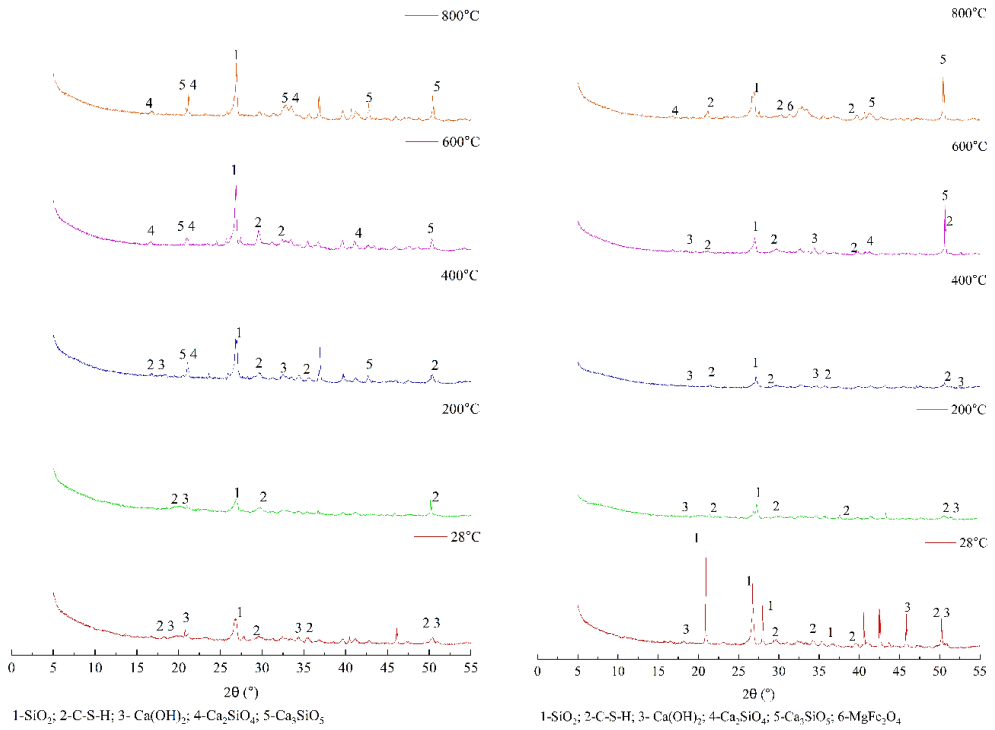

Fig. 16. XRD pattern for ECC at various temperatures: (a) E3, (b) E15

3.4.6 Microstructure at various temperatures

The microstructure of E3 and E15 at various temperatures is shown in Fig. 17. At 200^{0}C; both mixes show a change in the morphology of the fibres (Fig. 18). Therefore, PVA fibres Shrinking may result in matrix separation and a loss of strength. At 400^{0}C, when compared to the E3, the E15 exhibits a compacted matrix with a lower availability of unreacted FA.

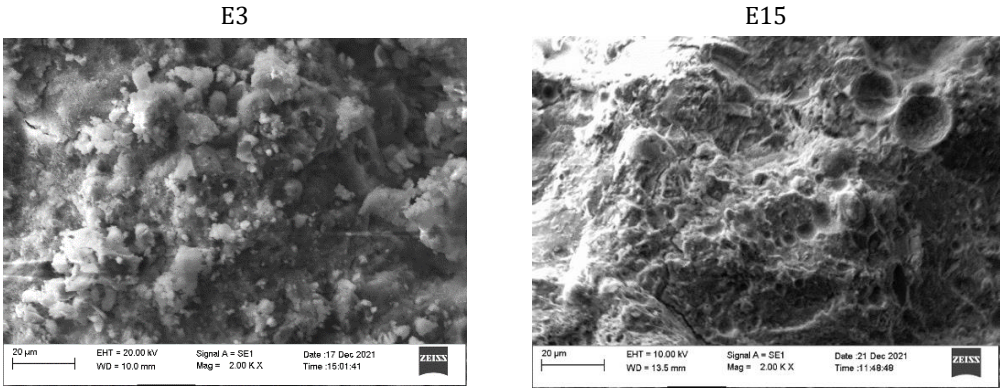

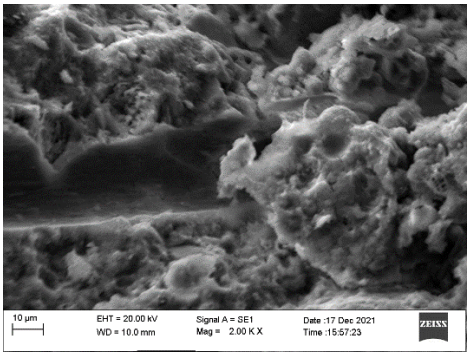

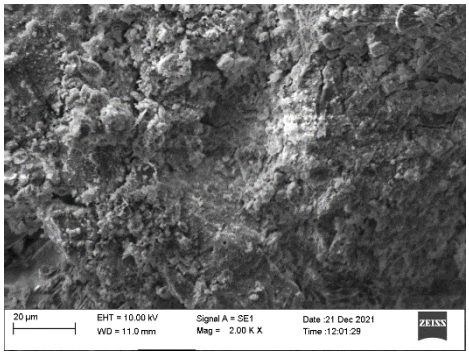

400^{0}C

(c) (d)

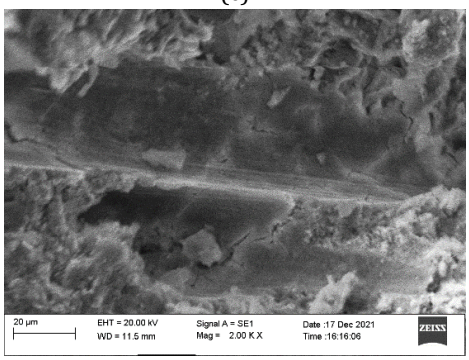

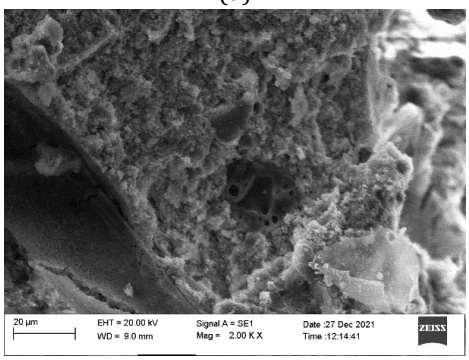

600^{0}C

(e) (f)

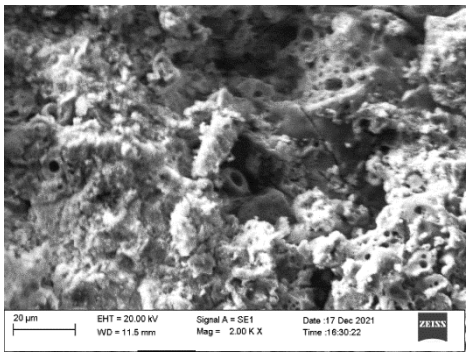

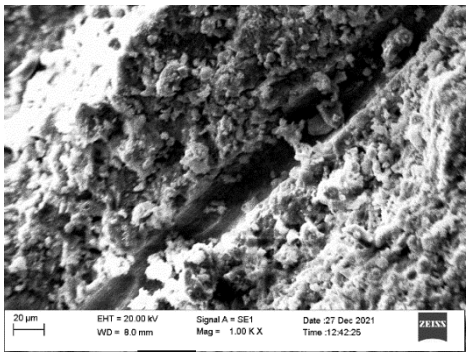

(g) (h)

800^{0}C

Fig. 17. Microstructure of E3 and E15 at various temperatures

In RS and SS ECC, the PVA fibres helped reduce pore pressure and prevent spalling through melting (seen in Fig. 9 and Fig. 19). At 600^{0}C, irregular bush-like structures are observed due to thermophysical reactions. Strength loss in both mixes occurred at 800^{0}C due to matrix deterioration, hydration product decomposition, and cracking. In contrast to E3, however, E15 exhibits a lesser loss in strength because of the denser structure and heat insulation capacity of the SS.

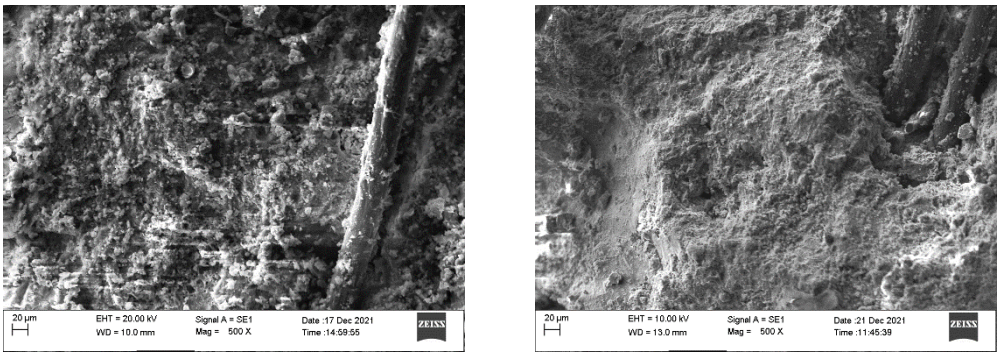

(a) (b)

Fig. 18. Shrinking of PVA fibres at 200^{0}C (a) E3 (b) E15

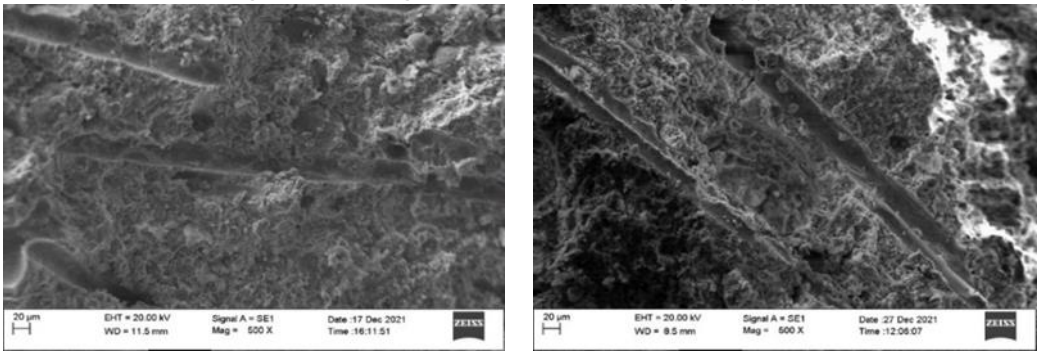

(a) (b)

Fig. 19. Melted PVA fibres after 400^{0}C (a) E3 (b) E15

4. Conclusions

The effect on the characteristics of ECC at elevated temperatures is experimentally studied. The following conclusions are formed in perspective with test findings:

- The reduction in flowability is observed when SS partially replaces the RS. The RS ECC mixes flowability is about 210-185 mm, and SS ECC mixes vary from 200-135 mm. Combining fibres with SS's angular and rough surface texture may restrict the smooth flow.
- The rise in compressive strength and UPV at all ages is observed with the replacement of the RS by SS up to 50%. Among all in the E15 mix, better improvements in strength and quality are noticed. $Ca(OH)_2$ produced on the hydration of cement can react with SiO_2 to form more C-S-H, which reduces the porosity and enhances the strength and quality.
- The spalling behaviour is not observed in both RS and SS ECC at elevated temperatures.
- The darker surface of RS ECC at 200^{0}C results from dehydration and water evaporation. As the temperature reaches 400^{0}C, PVA fibres melt, resulting in grey. After 600^{0}C, a light grey colour indicates C-S-H gel dehydration. Yellowish grey at 800^{0}C is related to C-S-H gel decomposition. Similarly, the colour of SS ECC specimens is comparable to that of RS ECC specimens up to 600^{0}C. Grey-white after exposure to 800^{0}C is due to ECC containing SS, which has higher heat-insulation capacity and extends the time it takes for hydration products to decompose.

- UPV test is used to understand the developments of voids and cracks in the ECC. The higher and lower values depend on the evolution of cracks in ECC. Thus, UPV tests have revealed that the E15 has better resistance to the evolution of cracks under elevated temperatures.
- The normalized strength of SS ECC is higher than that of RS ECC at elevated temperatures. The E15 specimens provided higher normalized strength even at the 800^0C.
- The higher peak stress and strain values are observed for E15 compared to E3 at various temperatures. The peak strain is relatively high at 28^0C because the PVA fibres prevent cracks from forming and expanding. The PVA fibres melted at 200^0C, increasing the porosity. As the temperature rises, more cracks form and the peak strain is attained at a higher rate.
- The XRD results revealed that The C-S-H phase is still identified at 800^0C for E15 and not observed for E3. At 800^0C, $MgFe_2O_4$ is found in E15.
- The SEM images showed that the increase in temperature, the voids and cracks increased in the RS ECC. However, at elevated temperatures, SS ECC retained a better-compacted structure than RS ECC due to the greater heat insulation capacity of the SS.

5. Future Scope

The performance of SS ECC reinforced with higher temperature-resistant fibres, including steel, carbon, and basalt fibres, should be studied. The durability property of hardened ECC in terms of volume stability has to be investigated.

Acknowledgement

The authors thank HIRA GODAWARI POWER & ISPAT, Sika India Pvt—Ltd, and Ultra Tech Cement for their support.

References

[1] Li Y, Li J, Yang EH, Guan X. Investigation of matrix cracking properties of engineered cementitious composites (ECCs) incorporating river sands. Cem Concr Compos. 2021;123(July):104204. https://doi.org/10.1016/j.cemconcomp.2021.104204

[2] Bahraq AA, Maslehuddin M, Al-Dulaijan SU. Macro- and Micro-Properties of Engineered Cementitious Composites (ECCs) Incorporating Industrial Waste Materials: A Review. Arab J Sci Eng. 2020;45(10):7869-95. https://doi.org/10.1007/s13369-020-04729-7

[3] Li VC, Bos FP, Yu K, McGee W, Ng TY, Figueiredo SC, et al. On the emergence of 3D printable Engineered, Strain Hardening Cementitious Composites (ECC/SHCC). Cem Concr Res. 2020;132(April):106038. https://doi.org/10.1016/j.cemconres.2020.106038

[4] Gu D, Pan J, Mustafa S, Huang Y, Luković M. Shear transfer mechanism in reinforced engineered cementitious composite (ECC) beams: Quantification of Vs and Vc. Eng Struct. 2022;261(April). https://doi.org/10.1016/j.engstruct.2022.114282

[5] Chung KL, Ghannam M, Zhang C. Effect of Specimen Shapes on Compressive Strength of Engineered Cementitious Composites (ECCs) with Different Values of Water-to-Binder Ratio and PVA Fiber. Arab J Sci Eng. 2018;43(4):1825-37. https://doi.org/10.1007/s13369-017-2776-8

[6] Liu JC, Tan KH. Mechanism of PVA fibers in mitigating explosive spalling of engineered cementitious composite at elevated temperature. Cem Concr Compos. 2018;93(May):235-45. https://doi.org/10.1016/j.cemconcomp.2018.07.015

[7] Lachemi M, Li VC. Effect of Fly Ash and PVA Fiber on Microstructural Damage and Residual Properties of Engineered Cementitious Composites Exposed to High Temperatures. 2011;23(December):1735-45. https://doi.org/10.1061/(ASCE)MT.1943-5533.0000335
[8] Sahmaran M, Lachemi M, Li VC. Assessing mechanical properties and microstructure of fire-damaged engineered cementitious composites. ACI Mater J. 2010;107(3):297-304. https://doi.org/10.14359/51663759
[9] Wang Z, Sun P, Zuo J, Liu C, Han Y, Zhang Z. Long-term properties and microstructure change of engineered cementitious composites subjected to high sulfate coal mine water in drying-wetting cycles. Mater Des. 2021;203:109610. https://doi.org/10.1016/j.matdes.2021.109610
[10] Zeng D, Cao M, Ming X. Characterization of mechanical behavior and mechanism of hybrid fiber reinforced cementitious composites after exposure to high temperatures. Mater Struct Constr. 2021;54(1):1-11. https://doi.org/10.1617/s11527-021-01622-z
[11] He J, Wang Q, Yao B, Ho J. Impact of Elevated Temperatures on the Performance of High-Strength Engineered Cementitious Composite. J Mater Civ Eng. 2021;33(9):1-17. https://doi.org/10.1061/(ASCE)MT.1943-5533.0003812
[12] Mohammed BS, Achara BE, Liew MS, Alaloul WS, Khed VC. Effects of elevated temperature on the tensile properties of NS-modified self-consolidating engineered cementitious composites and property optimization using response surface methodology (RSM). Constr Build Mater. 2019;206:449-69. https://doi.org/10.1016/j.conbuildmat.2019.02.033
[13] Cao K, Li H, Liu G, Huang Z, Wu G. Bonding properties between steel-basalt hybrid fibers reinforced cementitious composites and existing concrete at high temperatures. J Build Eng. 2023;70(December 2022):106371. https://doi.org/10.1016/j.jobe.2023.106371
[14] Chandru P, Karthikeyan J, Sahu AK, Sharma K, Natarajan C. Performance evaluation between ternary blended SCC mixes containing induction furnace slag and crushed stone as coarse aggregate. Constr Build Mater. 2021;267:120953. https://doi.org/10.1016/j.conbuildmat.2020.120953
[15] Chandru P, Karthikeyan J, Sahu AK, Sharma K, Natarajan C. z. Constr Build Mater. 2021;270:121483. https://doi.org/10.1016/j.conbuildmat.2020.121483
[16] Mehta PK. History and Status of Performance Tests for Evaluation of Soundness of Cements. Vol. STP 663, ASTM Special Technical Publication. 1978. p. 35-56. https://doi.org/10.1520/STP35785S
[17] Kabir H, Hooton RD, Popoff NJ. Evaluation of cement soundness using the ASTM C151 autoclave expansion test. Cem Concr Res. 2020;136(May). https://doi.org/10.1016/j.cemconres.2020.106159
[18] Dong Q, Wang G, Chen X, Tan J, Gu X. Recycling of steel slag aggregate in portland cement concrete: An overview. J Clean Prod. 2021;282:124447. https://doi.org/10.1016/j.jclepro.2020.124447
[19] Lun Y, Zhou M, Cai X, Xu F. Methods for improving volume stability of steel slag as fine aggregate. J Wuhan Univ Technol Mater Sci Ed. 2008;23(5):737-42. https://doi.org/10.1007/s11595-007-5737-3
[20] Hemalatha T, Sindu BS. Experimental Studies to Investigate Efficacies of Slag as Fine Aggregate Substitute. ACI Mater J. 2020;(117). https://doi.org/10.14359/51725981
[21] Agalit H, Zari N, Maaroufi M. Thermophysical and chemical characterization of induction furnace slags for high temperature thermal energy storage in solar tower plants. Sol Energy Mater Sol Cells. 2017;172(January):168-76. https://doi.org/10.1016/j.solmat.2017.07.035
[22] Netinger Grubeša I, Jelčić Rukavina M, Mladenovič A. Impact of High Temperature on Residual Properties of Concrete with Steel Slag Aggregate. J Mater Civ Eng. 2016;28(6):04016013. https://doi.org/10.1061/(ASCE)MT.1943-5533.0001515

[23] Liang X, Wu C, Su Y, Chen Z, Li Z. Development of ultra-high performance concrete with high fire resistance. 2018;179:400-12. https://doi.org/10.1016/j.conbuildmat.2018.05.241
[24] Jihad Miah M, Kawsar Ali M, Lo Monte F, Chandra Paul S, John Babafemi A, Šavija B. The effect of furnace steel slag powder on the performance of cementitious mortar at ambient temperature and after exposure to elevated temperatures. Structures. 2021;33(December 2020):2811-23. https://doi.org/10.1016/j.istruc.2021.06.047
[25] Li M, Li VC. Rheology, fiber dispersion, and robust properties of engineered cementitious composites. Mater Struct Constr. 2013;46(3):405-20. https://doi.org/10.1617/s11527-012-9909-z
[26] Nuaklong P, Worawatnalunart P, Jongvivatsakul P, Tangaramvong S, Pothisiri T, Likitlersuang S. Pre- and post-fire mechanical performances of high calcium fly ash geopolymer concrete containing granite waste. J Build Eng. 2021;44(July):103265.
[27] ISO:834. Fire-resistance tests- Elements of building construction. 1975;1975.
[28] Yang EH, Sahmaran M, Yang Y, Li VC. Rheological control in production of engineered cementitious composites. ACI Mater J. 2009;106(4):357-66. https://doi.org/10.14359/56656
[29] Abd El-Hakim RT, Elgendy GM, El-Badawy SM, Amin M. Performance evaluation of steel slag high performance concrete for sustainable pavements. Int J Pavement Eng. 2021;0(0):1-19.
[30] Li Q, Gao X, Xu S, Peng Y, Fu Y. Microstructure and Mechanical Properties of High-Toughness Fiber-Reinforced Cementitious Composites after Exposure to Elevated Temperatures. 2016;28(11):1-11. https://doi.org/10.1061/(ASCE)MT.1943-5533.0001647
[31] Zhuang X, Liang Y, Ho JCM, Wang YH, Lai M, Li X, et al. Post-fire behavior of steel slag fine aggregate concrete. Struct Concr. 2022;(September 2021):1-24.
[32] Erdem TK. Specimen size effect on the residual properties of engineered cementitious composites subjected to high temperatures. Cem Concr Compos. 2014;45:1-8. https://doi.org/10.1016/j.cemconcomp.2013.09.019
[33] Huang Z, Liew JYR, Li W. Evaluation of compressive behavior of ultra-lightweight cement composite after elevated temperature exposure. Constr Build Mater. 2017;148:579-89. https://doi.org/10.1016/j.conbuildmat.2017.04.121